A 2D½ model for low Prandtl number convection in an enclosure

V. Botton [a,*], R. Boussaa [a,b], R. Debacque [a], L. Hachani [b,c], K. Zaidat [b], H. Ben Hadid [a], Y. Fautrelle [b], D. Henry [a]

[a] *Laboratoire de Mécanique des Fluides et d'Acoustique, CNRS/Université de Lyon, Ecole Centrale de Lyon/Université Lyon 1/INSA de Lyon, ECL, 36 avenue Guy de Collongue, 69134 Ecully Cedex, France*
[b] *CNRS-SIMAP-EPM PHELMA, BP 75, 38402 Saint Martin d'Hères Cedex, France*
[c] *Laboratoire de Mécanique, Université Amar Telidji–Laghouat, Route de Ghardaia, BP 37G, Laghouat, Algeria*

Numerical simulations of stationary thermal convection in a differentially heated enclosure corre-sponding to the AFRODITE solidification benchmark experiment [1–5] are presented. The cavity of relative dimensions 10:6:1 (length:height:width) is characterized by a small transverse width. The Prandtl number Pr is varied within the range [0.0045, 0.03], typical of liquid metals, whereas the Grashof number, defined as $\mathrm{Gr} = g\beta(\Delta\theta/L)H^4/\nu^2$, is varied within the range $[1.3 \times 10^6, 1.6 \times 10^7]$. As shown by the reference 3D simulations, the temperature field in these situations is 2D (independent of the transverse direction); 2D simulations are, however, not able to catch the physics of the flow and the resulting temperature results are also erroneous. To improve these 2D simulation results while keeping reasonable computational times, a 2D½ model is developed, which will take into account the no-slip condition at the side walls. This model is obtained by averaging the governing equations over the width of the domain, with a transverse profile for the velocity featuring a uniform central part and two boundary layers of size δ (δ is fixed for the whole domain). The relative deviation of the temperature field between the 2D½ and 3D computations is investigated as a function of the Prandtl number, the Grashof number and the chosen boundary layer thickness. It is shown that an optimum value exists for δ, which gives a mean deviation in the middle plane of less than 2%, whereas the choice of a more usual parabolic profile would lead to a twice larger deviation. Good comparisons are also obtained with the original experi-mental results reported at the end of the paper. The 2D½ model is thus able to give results which compare well with fully 3D results. It can then be used for extensive parametric studies at a reasonable cost.

1. Introduction

Though computers run faster and faster, the extensive use of numerics for parametric studies still requires fast numerical models to be developed. In the present paper, we focus on the case of a narrow and horizontally elongated cavity in which a steady convection flow is driven by a steady horizontal, longitudinal heat flux (see configuration in Fig. 1). This geometry is chosen to correspond to the quasi-2D experimental benchmark for liquid metals directional solidification proposed by Fautrelle and co-workers (Ref. [1–5]), namely the AFRODITE experiment. The width is 10 mm, the height and length are respectively 60 mm and 100 mm; the imposed heat flux is along the longitudinal direction, $\boldsymbol{x_1}$. The 3D simulation of such a solidification problem is indeed costly, due in particular to the presence of a moving front in the problem: the solid–liquid interface. For a pure metal, the solid–liquid interface corresponds to an isotherm; being able to compute precisely, but cost-effectively, the temperature field in this configuration is thus of primary importance in this problem. As liquid metals are very low Prandtl-number fluids and the cavity is narrow, considering the temperature field to be 2D is a good approximation and the solidification problem by itself can be considered as a 2D problem. However, though the temperature is quasi uniform in the transverse direction $\boldsymbol{x_3}$, the velocity field cannot be uniform along $\boldsymbol{x_3}$ due to the no-slip condition at the walls. It is thus necessary to account for the three-dimensionality of the velocity field in order to solve the quasi-2D solidification problem. An alternative to fully 3D simulations is given by averaging the equations of mass, momentum and heat conservation along the $\boldsymbol{x_3}$ direction assuming a given shape for the velocity profile. Here, we investigate the ability of such a model to correctly predict the

* Corresponding author. Tel.: +33 4 72 43 70 19.
E-mail address: valery.botton@insa-lyon.fr (V. Botton).

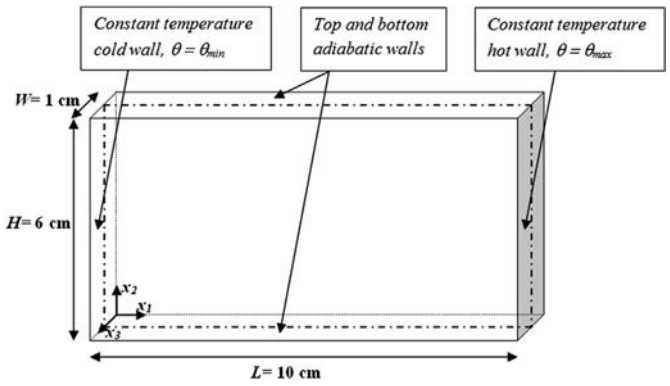

Fig. 1. Configuration of the study. The dashed-dotted line represents the vertical middle plane of the parallelepipedic cavity. The walls are adiabatic except the right and left side walls which are at a constant temperature, respectively hot and cold.

temperature field in the convection problem of Fig. 1. This is thus a first step towards proper solidification modelling which will be the subject of further studies; we consider this step as useful in the general framework of natural convection modelling.

Hele-Shaw [6] pointed out the interest of slender experimental configurations to get rid of inertia effects; by integrating the inertialess equations of motion over the transverse direction, he theoretically showed that, in such a configuration, the flow behaves like a potential flow. This approach is extensively described in textbooks; in particular, Schlichting and Gersten [7] pointed out that integrated inertia terms can be added in the approach, and Ockendon and Ockendon [8] indicate the possibility to apply this approach to solidification/melting problems. Since the work of Hele-Shaw [6], this method has been widely applied, both on the experimental and on the theoretical standpoints. It has not only been used in the investigation of potential flows but also in various studies related to instabilities [9,10], flows presenting interfaces [11,12], complex fluid flows [13], coupled problems [14–16], and modelling of industrial applications, such as continuous casting [17]. Note that, in the present paper, we will use the denomination "Hele-Shaw model" in the case where inertia is not accounted for and "2D½ model" when inertia terms are included in the integrated equations. Böckmann and Müller [14] used both a Hele-Shaw and a 2D½ formulation to model the progression of an autocatalytic front with a buoyancy driven instability. They found that the comparison with the experiment of Huang and Edwards [15] is far better with the 2D½ model than with the Hele-Shaw model. They however note that the agreement is still not perfect and that some ingredient may be missing. Katz and Worster [16] modelled a directional solidification experiment in an aqueous solution with the Hele-Shaw approach. They pointed out the ability of the model to reproduce chimney formation observed in the experiment. Such 2D½ models including inertia effects have also been used to investigate instabilities, for instance in a two-fluid parallel flow configuration [9] and in granular materials [13]. Note that Ruyer-Quil [10] includes this kind of model in the more general frame of weighted residual methods. Note finally that similar methods are extensively used under the denomination of shallow-water equations in the field of free surface hydraulics [18]. In all these papers, a parabolic velocity profile is assumed when integrating the equations of motion. This is clearly justified in the case of pressure driven duct flows, but the assumption is less clear in the case of buoyancy driven flows in a closed cavity, for example. In the following, we propose an alternative velocity profile and we show that its use leads to a better estimation of the temperature field in our configuration.

The boundary conditions are indicated in Fig. 1: all walls are adiabatic except the two endwalls ($x_1 = 0$ and $x_1 = 10$ mm), which both have a constant temperature ($\theta_{\min}$ and $\theta_{\max}$ respectively). The cold endwall is on the left hand side of the figure, so that the flow is expected to be directed along $\boldsymbol{x_1}$ in the lower part of the cavity and along $-\boldsymbol{x_1}$ in the upper part.

The simulations are performed using the StarCCM+ commercial CFD software. A regular grid with $125 \times 75 \times 25$ cells has been used for the 3D computations. It has been checked that refinement of the grid did not change the results significantly (see the comments at the end of the section). Unless specified, a steady segregated solver has been used. The convective terms were discretized using a second order upwind scheme. Convergence is considered to be reached when all residuals have decreased at least by a factor 10^3 compared to the first 5 iterations (see Fig. 7 for a typical convergence curve). In addition, the maximum velocity in the vertical middle plane is monitored in order to check it has reached a constant value. In the absence of experimental velocity measurements in this configuration, the 3D computations have been confronted with other 3D computations performed with drastically different methods: a spectral element method using Legendre polynomials at the Gauss–Lobatto discretization points, and a simulation by Lattice-Boltzmann algorithm. We have verified that the difference in maximum velocity components over the fluid domain is less than 1% between these computations. In the following, we will consider the 3D computations using the StarCCM+ software as a reference case since we have implemented our 2D½ model in this software: this will allow a proper comparison, not only in terms of quantitative results, but also in terms of computational time. Some purely 2D simulations are also reported in this paper; what is referred to as a purely 2D approximation is to assume that all fields are functions of $\boldsymbol{x_1}$ and $\boldsymbol{x_2}$ only and that the velocity component along $\boldsymbol{x_3}$ is zero. These simulations have been made on a 125×75 grid, which corresponds to the mesh used in the vertical middle plane of the 3D computations.

As the geometry is fixed and the problem is steady, the only parameters are the Grashof number and the Prandtl number defined as:

$$\mathrm{Gr} = \frac{g\beta(\Delta\theta/L)H^4}{\nu^2}, \tag{1}$$

and

$$\mathrm{Pr} = \frac{\nu}{\alpha}, \tag{2}$$

where β, ν and α are respectively the thermal expansion coefficient, the kinematic viscosity and the thermal diffusivity; $\Delta\theta$ is the temperature difference between the hot and the cold walls: $\Delta\theta = \theta_{\max} - \theta_{\min}$.

The sensitivity of the simulation to the mesh has been tested by progressively refining the cell dimensions from one mesh to another by a factor 2 in the three directions. The coarser mesh has $25 \times 15 \times 5$ cells versus $400 \times 240 \times 80$ for the finer mesh; five meshes where thus tested, in addition to the mesh used in the study, which had $125 \times 75 \times 25$ elements. The case used for this test is a 3D stationary simulation with $\mathrm{Gr} = 4.34 \times 10^6$, $\mathrm{Pr} = 0.0129$. We have chosen to compare the different solutions with regard to their ability to predict the longitudinal temperature and velocity profiles along the middle axis parallel to $\boldsymbol{x_1}$. The 25 points corresponding to the coarser mesh also belong to the other meshes; these points were thus used to compute an estimate of the deviation with respect to the results obtained on the finer mesh, which was considered as the reference case. The following formulas have

Table 1
Sensitivity of the 3D simulations to mesh refinement. Test based on the longitudinal velocity and temperature profiles at mid-position. The simulation corresponds to $Gr = 4.34 \times 10^6$ and $Pr = 0.0129$.

Cells number (length:height:width)	Velocity deviation in %	Temperature deviation in %
$25 \times 15 \times 5$	6.977	1.867
$50 \times 30 \times 10$	1.188	0.111
$100 \times 60 \times 20$	0.996	0.0145
$200 \times 120 \times 40$	0.304	0.0030
$400 \times 240 \times 80$	0	0

been used to assess the velocity magnitude deviation and the temperature deviation, respectively:

$$\Delta^{u}_{\text{mesh}} = \frac{1}{25}\sum_{i=1}^{25}\left|\frac{u_i^{\text{tested}} - u_i^{\text{reference}}}{\max\left(u_i^{\text{reference}}\right)}\right|, \tag{3}$$

$$\Delta^{\theta}_{\text{mesh}} = \frac{1}{25}\sum_{i=1}^{25}\left|\frac{\theta_i^{\text{tested}} - \theta_i^{\text{reference}}}{\Delta\theta}\right|, \tag{4}$$

where u and θ denotes the velocity magnitude and the temperature, respectively, and the superscript *tested* and *reference* refer to the tested mesh and the reference mesh, respectively. The results of this test are shown in Table 1. We see a very good convergence of the results when the mesh is refined. For the mesh used in the present investigation ($125 \times 75 \times 25$ elements) the error is less than 1% for the velocity and less than 0.014% for the temperature. The convergence for the temperature is far better than for the velocity; this can be attributed to the low value of the Prandtl number and to the sharpness of the velocity profiles near their extrema. As our main objective is to get a well estimated temperature field, we have considered that the grid with $125 \times 75 \times 25$ cells offers a very good precision together with reasonable computational times. Note that the same test conducted for the 2D1/2 simulations gives still better results.

2. The limits of pure 2D modelling

Fig. 2a shows a typical solution obtained through a purely 2D simulation of the problem with $Gr = 1.296 \times 10^6$ and $Pr = 0.0129$. The colours (or grey levels) are isovalues of the velocity magnitude and the lines are isotherms. This picture can be compared to Fig. 2b showing the vertical middle plane solution extracted from a 3D simulation performed in the same conditions. As can be seen, there is a drastic difference in the velocity field and temperature field shape. The velocity field computed from a 2D model indeed exhibits a so-called "flying wheel" structure, while a more elongated Hadley circulation, which occupies the whole fluid domain, is obtained from the 3D computations. In addition, the flow turns out to be steady in the case of the 3D simulation while it is unsteady in the 2D simulation. It is thus clear that the 2D model does not catch the physics of this configuration that is confined in the transverse $\boldsymbol{x_3}$ direction.

For a ten times higher Grashof number, $Gr = 1.296 \times 10^7$, Fig. 3a and b show that the same difference, though less obvious, is still present between the two structures obtained through the 2D and the 3D simulations. The difference is attenuated by the fact that the "flying wheel" is less circular and occupies more space in this elongated domain, but we still obtain an unsteady solution in the 2D simulation and a steady solution in the 3D simulation.

As a conclusion, it is clearly not possible to rely on a purely 2D approximation of the problem to save computation time since the effects of the no-slip condition at the lateral walls is of primary importance in this problem. It is all the more a shame as the temperature profiles in the transverse direction are indeed almost uniform, as can be seen in the upper view of Fig. 4 showing isotherms in a plane of constant x_2. Fig. 4 also gives a qualitative view of the velocity variations along the $\boldsymbol{x_3}$ direction in this plane.

3. Theoretical basis of our 2D½ model

A way of saving computational time without renouncing to take into account the no-slip condition at the lateral walls is to average the equations of the problem along the transverse $\boldsymbol{x_3}$ direction. The averaging is made analytically, assuming an arbitrary shape for the transverse velocity, pressure and temperature profiles. This leads to formulations often referred to as Hele-Shaw models, Saint-Venant/shallow-water models in the framework of free surface hydraulics, or more generally 2D½ models. We recall hereunder the derivation of these models and the assumptions made in the present work concerning the transverse variation of velocity, pressure and temperature.

Let us start from the local mass, momentum and heat conservation equations for a Newtonian incompressible fluid under the Boussinesq approximation:

$$\begin{cases} \dfrac{\partial u_i}{\partial t} + \vec{u}.\overrightarrow{\text{grad}}\, u_i = -\dfrac{\partial p}{\partial x_i} + A_L \text{Gr} T \delta_{i,2} + \Delta u_i \quad \text{for } i = 1,\ 2 \text{ and } 3, \\ \text{div}\ \vec{u} = 0, \\ \dfrac{\partial T}{\partial t} + \vec{u}.\overrightarrow{\text{grad}}\, T = \text{Pr}\Delta T, \end{cases} \tag{5}$$

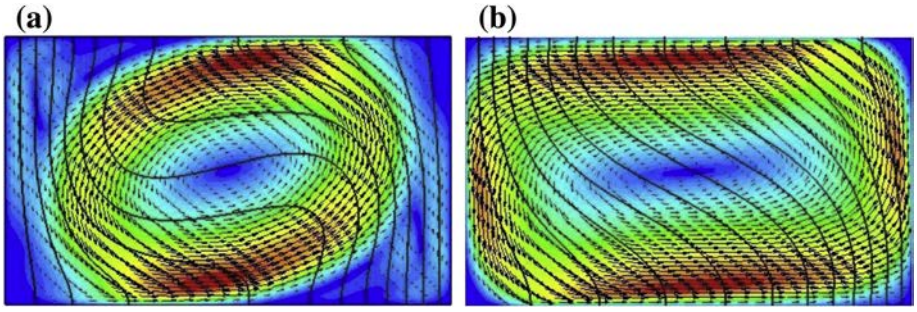

Fig. 2. Qualitative view of the velocity field (vectors and colours/grey levels) and temperature field (isolines) for $Gr = 1.296 \times 10^6$ and $Pr = 0.0129$. On the left (2.a): snapshot of the 2D unsteady solution; on the right (2.b): 3D stationary solution in the vertical middle plane. (For interpretation of the references to colour in this figure legend, the reader is referred to the web version of this article.)

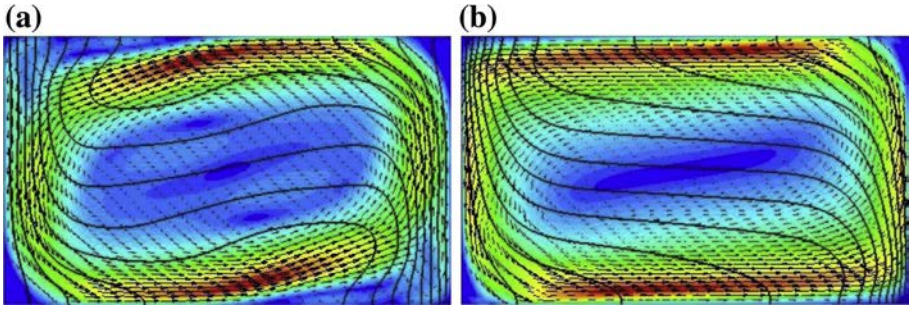

Fig. 3. Qualitative view of the velocity field (vectors and colours/grey levels) and temperature field (isolines) for $\mathrm{Gr} = 1.296 \times 10^7$ and $\mathrm{Pr} = 0.0129$. On the left (3.a): snapshot of the 2D unsteady solution; on the right (3.b): 3D stationary solution in the vertical middle plane. (For interpretation of the references to colour in this figure legend, the reader is referred to the web version of this article.)

where $\delta_{i,j}$ is the Kronecker symbol, A_L is the longitudinal aspect ratio, $A_L = L/H$, which is fixed to $A_L = 5/3$ in the present work. The non-dimensional form of the equation has been obtained by using ν/H as a characteristic velocity, H as a characteristic length whatever the considered direction, H^2/ν as a characteristic time and $\rho\,(\nu/H)^2$ as a characteristic pressure. The dimensionless temperature is calculated as:

$$T = \frac{\theta - \frac{1}{2}(\theta_{\max} + \theta_{\min})}{(\theta_{\max} - \theta_{\min})}, \tag{6}$$

where θ, $\theta_{\min}$ and $\theta_{\max}$ denote the dimensional temperature at any location in the fluid domain, on the left boundary and on the right boundary, respectively. In addition to the no-slip condition for the velocity at the walls, the thermal boundary conditions are then:

$$T = -\tfrac{1}{2} \text{ at the left wall}, \tag{7}$$

$$T = \tfrac{1}{2} \text{ at the right wall}, \tag{8}$$

$$\mathrm{d}T/\mathrm{d}n = 0 \text{ at the other walls}, \tag{9}$$

d./dn denoting derivation along the direction normal to the wall.

In the following, we rely on the boundary condition (9) and on the small values of both the cavity width and the Prandtl number to assume that the transverse temperature profiles are uniform (see the upper plot in Fig. 4). We also assume that both the pressure and the velocity fields can be described as the product of a function of x_3 only, which gives the shape of the transverse profile, and a function of x_1 and x_2, which accounts for the variations of these fields in longitudinal vertical planes. This separation of variables is written as:

$$\begin{cases} T(x_1,x_2,x_3,t) = \overline{T}(x_1,x_2,t), \\ u_i(x_1,x_2,x_3,t) = \overline{u_i}(x_1,x_2,t) f(x_3) \quad \text{for } i = 1 \text{ and } 2, \\ u_3 = 0, \\ p(x_1,x_2,x_3,t) = \overline{p}(x_1,x_2,t) g(x_3), \\ \dfrac{1}{A_w}\displaystyle\int_0^{A_w} f(x_3)\mathrm{d}x_3 = 1 \quad \text{and} \quad \dfrac{1}{A_w}\int_0^{A_w} g(x_3)dx_3 = 1, \end{cases} \tag{10}$$

where A_w is the transverse aspect ratio, $A_w = W/H$. Substitution into the 3D conservation equations system (5) and integration along $\boldsymbol{x_3}$ yield:

$$\begin{cases} \dfrac{\partial \overline{u}_i}{\partial t} + \overrightarrow{\overline{u}}.\overrightarrow{\mathrm{grad}}\,\overline{u}_i = -\dfrac{\partial \overline{p}}{\partial x_i} + A_L \mathrm{Gr} T \delta_{i,2} + \Delta \overline{u}_i + S_i \quad \text{for } i = 1 \text{ and } 2, \\ \mathrm{div}\,\overrightarrow{\overline{u}} = 0, \\ \dfrac{\partial \overline{T}}{\partial t} + \overrightarrow{\overline{u}}.\overrightarrow{\mathrm{grad}}\,\overline{T} = \mathrm{Pr}\Delta\overline{T}, \\ S_i = \left[1 - \dfrac{1}{A_w}\displaystyle\int_0^{A_w} f^2(x_3)\mathrm{d}x_3\right] \overrightarrow{\overline{u}}.\overrightarrow{\mathrm{grad}}\,\overline{u}_i + \dfrac{1}{A_w}\left[\dfrac{\partial f}{\partial x_3}\right]_0^{A_w} \overline{u}_i, \end{cases} \tag{11}$$

where every variable is a function of x_1, x_2 and t only. The gradient and Laplacian operators can thus be replaced by their 2D counterparts. The obtained system then takes the form of the usual plane 2D formulation featuring an additional source term $\boldsymbol{S}$ in the momentum equation. This source term can be expressed analytically after choosing an adequate velocity profile shape. The most often used profile is the Poiseuille parabolic profile ($f(x_3) = 6/A_w^2(A_w - x_3)x_3$), for this corresponds to the established flow driven by a uniform volumetric force. In this case, the source term takes the following form:

$$S_{P,i} = -\frac{1}{5}\overrightarrow{\overline{u}}.\overrightarrow{\mathrm{grad}}\,\overline{u}_i - \frac{12}{A_w^2}\overline{u}_i. \tag{12}$$

However, as can be seen in the upper view of Fig. 4 featuring 3D computation results, the transverse velocity profiles in the real 3D situations are very different from parabolic profiles. These profiles

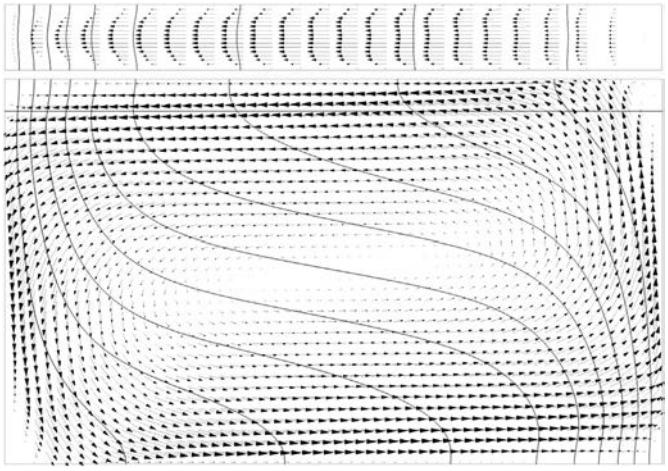

Fig. 4. Qualitative views of the velocity and temperature fields obtained from a 3D computation ($\mathrm{Gr} = 4.34 \times 10^6$ and $\mathrm{Pr} = 0.0129$) in the vertical middle plane (lower view) and in a horizontal plane (upper view). The vectors represent the velocity field. The lines are isotherms, except the horizontal straight line in the lower view, which gives the location of the horizontal cross section represented in the upper view.

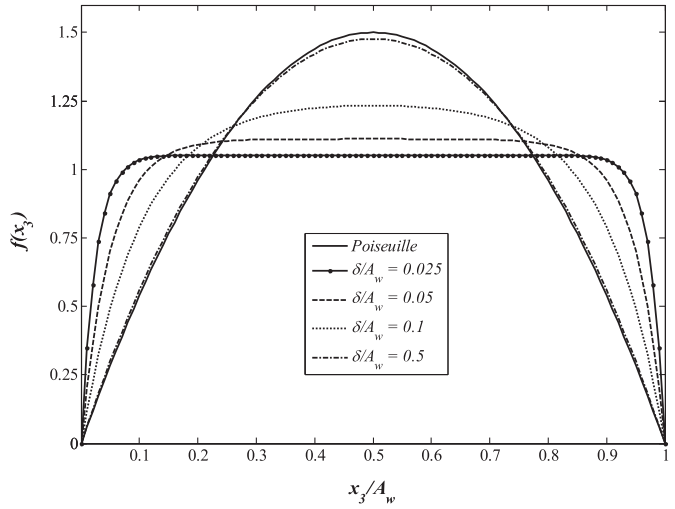

Fig. 5. Different types of profiles used to model the transverse variation of the velocity in our transversally confined cavity: Poiseuille profile (parabolic) and Hartmann-type profiles (13) for different values of δ.

rather exhibit marked boundary layers along the walls and a nearly uniform bulk velocity. Such profiles can be better described by the following relation:

$$f(x_3) = F\left[1 - \frac{\cosh\left(\dfrac{x_3 - A_w/2}{\delta}\right)}{\cosh\left(\dfrac{A_w}{2\delta}\right)}\right] \quad \text{with } F = \frac{1}{1 - \dfrac{2\delta}{A_w}\tanh\left(\dfrac{A_w}{2\delta}\right)}, \tag{13}$$

where δ is an arbitrary length. As shown in Fig. 5, for small values of δ, typically $\delta < A_w/10$, these profiles, which feature a quite uniform bulk velocity surrounded by two boundary layers of typical size δ, mimic quite well the 3D profiles. In the following, we will denote these profiles as "Hartmann-type profiles" in reference to the well-known solution of MHD duct flows [19].

For such Hartmann-type profiles, the source term in (11) becomes:

$$S_{H,i} = \left\{1 - F^2\left[\frac{3}{2} - \frac{1}{2}\tanh^2\left(\frac{A_w}{2\delta}\right) - \frac{3\delta}{A_w}\tanh\left(\frac{A_w}{2\delta}\right)\right]\right\} \times \overrightarrow{\overline{u}}.\overrightarrow{\text{grad}}\,\overline{u}_i - F\left[\frac{2}{\delta A_w}\tanh\left(\frac{A_w}{2\delta}\right)\right]\overline{u}_i. \tag{14}$$

Note that if δ is greater than $A_w/2$, the Hartmann-type profiles approach the Poiseuille profile very closely, and the Poiseuille profile is reached asymptotically for $\delta \to \infty$.

4. Comparison between 3D and 2D½ computations

In this section, we want to show that the 2D½ computations, with the Hartmann-type model presented in the previous section, can accurately reproduce 3D results. The boundary layer thickness value δ is an adjustable parameter within a reasonable range. This value can be optimized with respect to 3D numerical, theoretical or experimental results. In the following the optimization will be made with respect to 3D computations. Our objective is to show the interest of such 2D½ models to perform parametric studies at a reasonable cost: one or a few 3D simulations are necessary to adjust the value of δ for the given range of parameters (Gr and Pr) after what an extensive parametric study with the 2D½ model can then be performed.

A qualitative illustration of the ability of this model to give a better prediction than a 2D computation is given in Fig. 6. Velocity vectors and isotherms plotted in this figure are computed using the Poiseuille profile (left) and the Hartmann-type profile (right). These results can be compared to the purely 2D and 3D results of Fig. 3 since Gr and Pr have the same values. The physics of the flow is obviously better captured by these two models than by the purely 2D model, while the computation time is typically the same: 8 min on a standard PC, instead of 3 h in the case of a 3D computation. Note that no steady solution is found with the 2D½-Poiseuille model and that a recirculation in the upper-left and lower-right corner is present as in the 2D simulations. This recirculation is present neither in the 3D nor in the 2D½-Hartmann models, which both exhibit a steady solution; this denotes the better ability of this last model to account for inertia effects.

Typical convergence curves for the residuals obtained in the computation of a steady solution with the 2D½-Hartmann model are plotted in Fig. 7; reasonable convergence is reached after 2500 iterations. In the present results, 5000 iterations have arbitrarily been used. The monitoring of the velocity value in 3 points of the domain shows that typical variations after 1000 iterations concern the fifth decimal only.

Our quantitative approach to compare the quality of different solutions with respect to the 3D solution is based on the ability to predict the temperature field. We thus define the following estimators of the difference between a 2D½ solution and the 3D solution in the vertical middle plane:

$$\Delta_{\text{mean}} = \frac{1}{n}\sum_{i=1}^{n}\left|T_i^{2D\,1/2} - T_i^{3D}\right|, \tag{15}$$

and

$$\Delta_{\max} = \max_i\left|T_i^{2D\,1/2} - T_i^{3D}\right|, \tag{16}$$

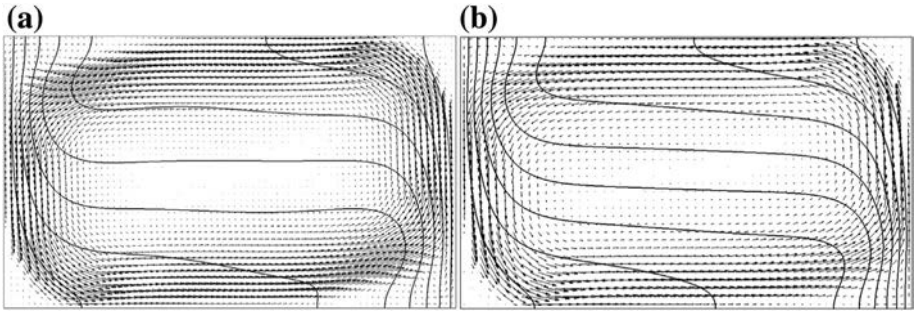

Fig. 6. Qualitative view of the velocity field (vectors) and isotherms for $\text{Gr} = 1.296 \times 10^7$ and $\text{Pr} = 0.0129$. Left hand-side: 2D-½ Poiseuille model (snapshot of the unsteady solution); right hand-side: 2D-½ Hartmann model with $\delta = 0.15\ A_w$ (steady solution).

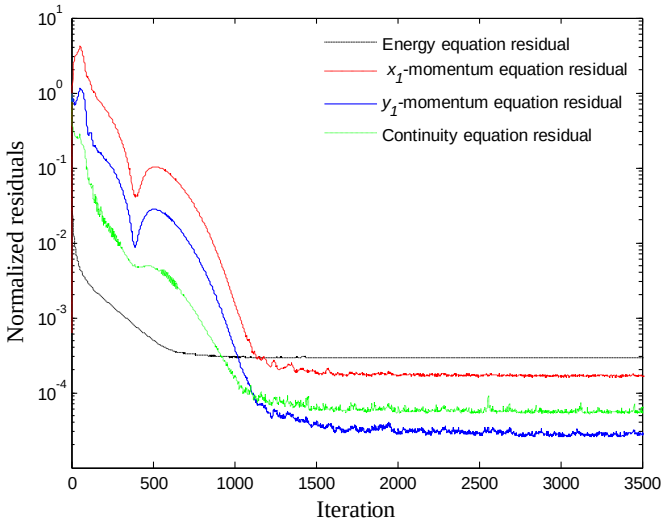

Fig. 7. Typical residual convergence curves for the computation of a steady solution with the 2D½-Hartmann model, here for Gr = 4.34 × 10^6 and Pr = 0.0129.

where n is the number of cells in the 2D mesh (note that the mesh used in the 2D½ simulations coincides with that of the 3D case in the vertical middle plane). Let us recall that, in this non dimensional description of the problem, the temperature variation between the hot and the cold walls is 1 so that the estimators will be expressed in percent of the overall temperature difference, $\Delta\theta$.

The value of the thickness δ is a free parameter in the 2D½-Hartmann model. However for each couple of parameter (Gr, Pr), the mean and maximum deviations with respect to the 3D computation can be expected to feature a minimum for some value of δ. This is illustrated in Fig. 8 showing Δ_{max} and Δ_{mean} as a function of δ/A_w for two arbitrary couples (Gr, Pr) = (4.34 × 10^6, 0.0129) and (Gr, Pr) = (1.296 × 10^7, 0.0047). It appears that the 2D½ versus 3D deviation can be drastically reduced by choosing an appropriate value of the boundary layer thickness. The minimum mean deviation is indeed less than 1%. The "best-value" for δ is found to be a function of Pr and Gr; in the case where a value of δ has to be selected to investigate a given range of parameters, the chosen value is thus necessarily a compromise. In the present parameters range, a value of $\delta = 0.15\ A_w$ seems appropriate and will be systematically used in the following.

Fig. 9 shows the mean deviation, Δ_{mean}, and maximum deviation, Δ_{max}, of the 2D½ simulations with respect to the 3D case, plotted as a function of the Prandtl number for Gr = 4.34 × 10^6. Solid and open symbols are for Δ_{mean} and Δ_{max} respectively. Circles represent results obtained assuming a Poiseuille profile while diamonds correspond to results obtained assuming a Hartmann-type profile with a boundary layer thickness $\delta = 0.15\ A_w$. It is clear from this picture that assuming a Hartmann-type profile rather than a Poiseuille profile significantly improves the model since the deviation is generally divided by more than 2. For this value of the Grashof number, the mean deviation is smaller than 1%, while the maximum deviation over the domain is generally less than 3%. In addition to these values, Fig. 10 gives a typical map of the deviation, obtained for Pr = 0.0129. We see that the region of high deviation corresponds to the regions where the flow exhibits a separation from the wall and a recirculation. This illustrates that the efficiency of this type of model is linked to its ability to predict the convection heat transfer in the corners of the cavity.

The variations of the 2D½ versus 3D deviations as a function of the Grashof number are plotted in Fig. 11 for Pr = 0.0129. A minimum is found around Gr = 4.34 × 10^6 and a nearly linear increase is observed for higher values of Gr. Above Gr = 10^7, the maximum deviation in the domain exceeds 5%, and approaches 10% for Gr = 1.626 × 10^7; we thus consider our model to be valid in this range of parameters since this deviation is of the same order of magnitude as experimental measurements uncertainty. Note that these values are local maxima and the mean deviation remains small, with values below 1.5%. As the minimum Gr number tested in the present study is 1.296 × 10^6, we can consider the model to be valid over more than one decade in terms of Grashof number.

5. 2D½ numerical results compared to experiment

Experimental results have been obtained with the experimental setup described in Refs. [3–5]. In these references, tin–lead alloys

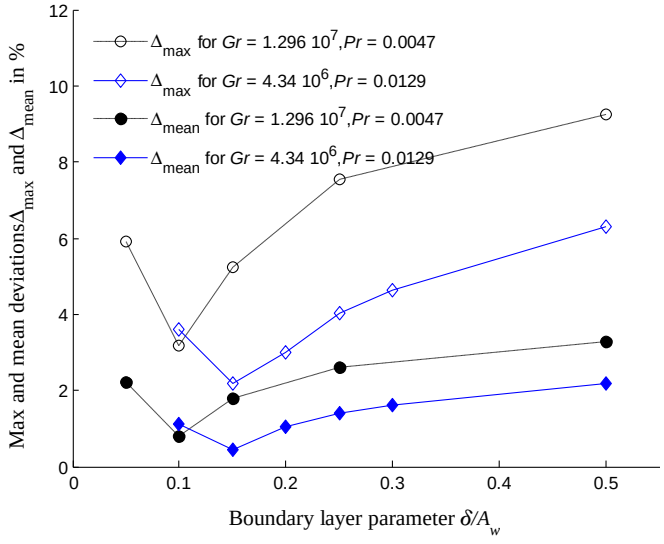

Fig. 8. Normalized maximum (Δ_{max}) and mean (Δ_{mean}) temperature deviations (in %) of the 2D½-Hartmann simulations with respect to the 3D simulation as a function of the boundary layer parameter δ/A_w. The two reported cases correspond to Gr = 4.34 × 10^6, Pr = 0.0129 and Gr = 1.296 × 10^7, Pr = 0.0047.

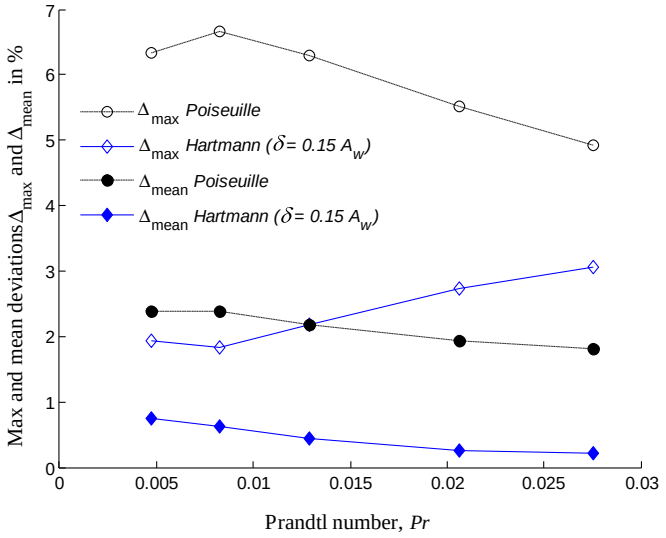

Fig. 9. Normalized maximum (Δ_{max}) and mean (Δ_{mean}) temperature deviations (in %) of the 2D½ simulations with respect to the 3D simulations as a function of the Prandtl number for Gr = 4.34 × 10^6. Circles and diamonds correspond to 2D½ models featuring Poiseuille and Hartmann-type ($\delta = 0.15\ A_w$) profiles, respectively; solid symbols are for Δ_{mean} and open symbols for Δ_{max}.

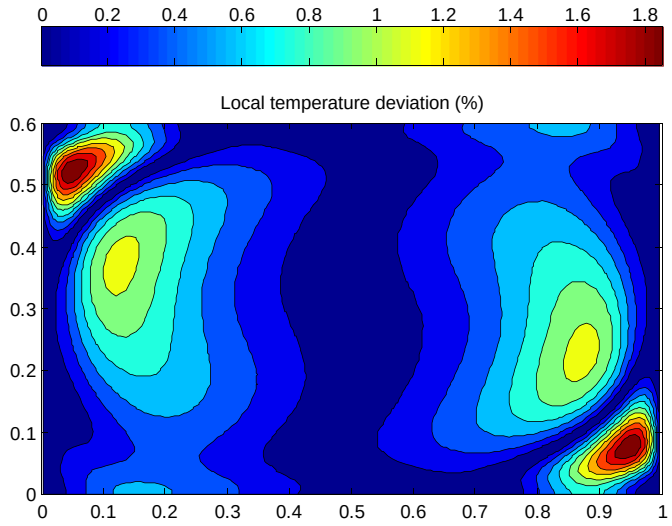

Fig. 10. Normalized deviation between the temperature field in the middle plane of a 3D simulation and the temperature field obtained from a 2D½-Hartmann simulation with $\delta = 0.15\ A_w$ for $\mathrm{Gr} = 4.34 \times 10^6$ and $\mathrm{Pr} = 0.0129$.

solidification experiments are reported. In contrast, our experiments will concern pure tin samples in liquid state and no solidification will be considered. The experimental cavity (defined in Fig. 1) is heated via two heat exchangers placed along the end-walls. Once the metal is liquid, a temperature difference is applied between these end-walls (cold temperature at $x_1 = 0$ and hot temperature at $x_1 = 10$ cm), and a convective steady state is obtained. The temperature distribution over the front side wall ((x_1,x_2)-plane at $x_3 = 10$ mm) can be obtained with an array of 50 copper constantan (type K) thermocouples, and comparisons with the numerical results on these temperature values are then possible.

In the experiment, only the temperature difference between the two heat exchangers is monitored, and the temperature difference in the liquid $\Delta\theta$, which is needed for the comparisons with the numerical simulations, is unknown, though it is expected to be

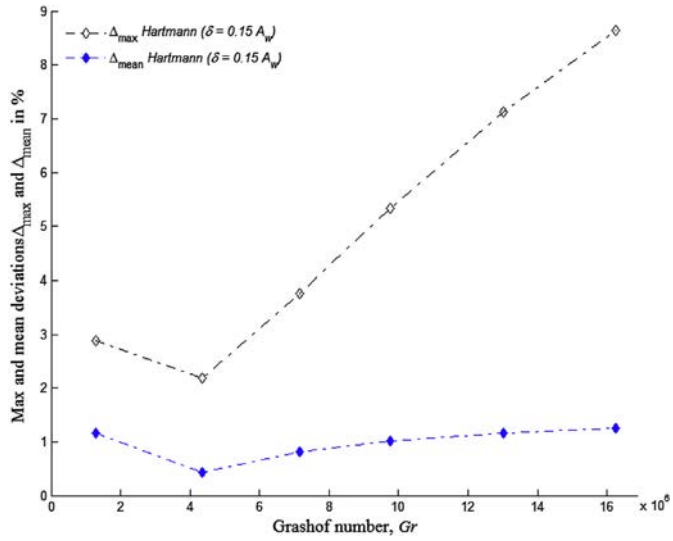

Fig. 11. Normalized maximum (Δ_{max}) and mean (Δ_{mean}) temperature deviations (in %) of the 2D½-Hartmann model, with $\delta = 0.15\ A_w$, with respect to the 3D simulations as a function of the Grashof number for $\mathrm{Pr} = 0.0129$. Solid symbols are for Δ_{mean} and open symbols for Δ_{max}.

Table 2
Thermophysical parameters of pure liquid tin (Sn) [20].

Density	kg m^{-3}	7000
Specific heat	J kg^{-1} C^{-1}	243
Dynamic viscosity	kg m^{-1} s^{-1}	0.002
Thermal conductivity	W m^{-1} C^{-1}	32
Thermal expansion coefficient	K^{-1}	9.5×10^{-5}

significantly smaller because of thermal resistances. To have an estimation of $\Delta\theta$, the temperature of the melt near the two end-walls will be determined. For that, the heat conservation law is applied, along the longitudinal direction $\boldsymbol{x_1}$ at mid-height, to a control volume containing two thermocouples in the heat exchanger (measuring the temperatures θ_{H1} and θ_{H2}) and one in the melt (measuring θ_{M1}). If $\theta_{endwall}$ is the unknown temperature along the endwall, following what is proposed in Refs. [3–5], we can write:

$$\phi = \frac{\lambda_{Cu}(\theta_{H1} - \theta_{H2})}{e_1} = \frac{\lambda_{Sn}(\theta_{endwall} - \theta_{M1})}{e_2}. \quad (17)$$

Where λ_{Cu} and λ_{Sn} are the thermal conductivities of solid copper and liquid tin, equal to 380 and 32 W m^{-1} K^{-1} respectively, $e_1 = 15$ mm is the horizontal distance between the exchanger thermocouples, and $e_2 = 5$ mm is the horizontal distance between the thermocouple $M1$ and the end-wall. This calculation is performed for both end-walls and a temperature difference $\Delta\theta = 6$ K is thus obtained. Using this value and the thermophysical parameters of Table 2 [20], we evaluate the following dimensionless parameter values: $\mathrm{Gr} = 8.9 \times 10^6$ and $\mathrm{Pr} = 0.0152$, which belong to the ranges studied in the previous sections.

These parameters have been used in 2D, 2D½ and 3D simulations. The Hartmann model with $\delta/A_w = 0.15$ was chosen for the 2D½ simulation. The comparison between the experimental and numerical results is shown in Fig. 12, where the longitudinal temperature profile along $\boldsymbol{x_1}$ at mid-height is plotted. We see that the 3D and 2D½ numerical profiles are very close to the experimental values of the temperature. In contrast, the profile obtained in the 2D simulation is too much deformed by the flow. This causes an inversion of the thermal gradient in the centre of the cavity, which is neither observed in the experiment nor obtained in the 2D½ and 3D simulations results.

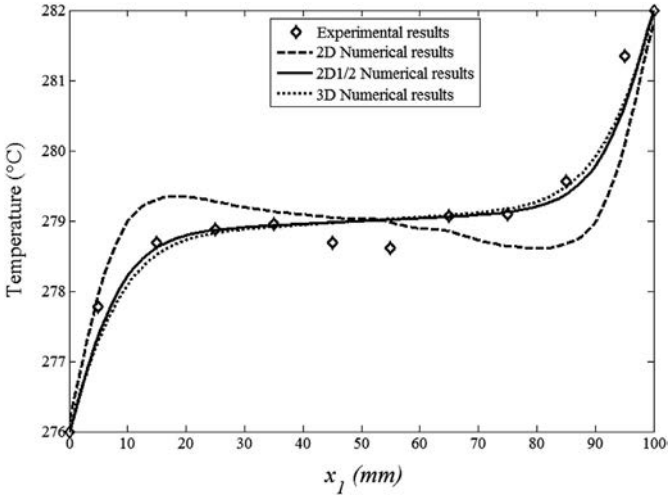

Fig. 12. Temperature profiles along $\boldsymbol{x_1}$ at mid-height of the cavity ($x_2 = 30$ mm) for the numerical and experimental results ($\mathrm{Gr} = 8.88 \times 10^6$ and $\mathrm{Pr} = 0.0152$). The Hartmann model with $\delta/A_w = 0.15$ is used for the 2D½ simulations.

Using the temperature at the 50 positions of the thermocouples, we can also define the relative deviation, $\Delta_{num/exp}$, between the numerical and experimental results:

$$\Delta_{num/exp} = \frac{1}{50}\sum_{i=1}^{50}\left|\frac{\theta_i^{num} - \theta_i^{exp}}{\Delta\theta}\right|. \quad (18)$$

The relative deviation with respect to the experimental results is 5.26%, 5.39% and 8.32% for the 3D, 2D½ and 2D results, respectively. We see that the best approximation is still obtained by the 3D and 2D½ models which give similar deviations. It can be concluded that the 2D½ simulations (as well as the 3D simulations) are able to describe the physics of the experiment with a good approximation.

6. Conclusion

We have presented a 2D½ model for thermal convection in a rectangular differentially heated cavity. The geometry has been chosen to correspond to a solidification benchmark experiment by Fautrelle and co-workers [1–5]. The dimension of the cavity in the horizontal transverse direction, $\boldsymbol{x_3}$, is one order of magnitude smaller than the dimensions in the other directions (direction of the horizontal heat-flux, $\boldsymbol{x_1}$, and vertical direction, $\boldsymbol{x_2}$). As the considered liquid is metallic, the temperature field can be expected to be uniform in this transverse direction, $\boldsymbol{x_3}$, but this is not the case for the velocity field which fulfils no-slip conditions at the walls. Fully 2D models thus poorly catch the physics of the flow since they are far less dissipative than the real case. We give an illustrative case in which the structure of the flow is poorly recovered by the 2D model and in which no steady solution is found with the 2D model while a steady solution is reached in the 3D simulation. On the other hand, fully 3D computations are highly time consuming and so, not easy to perform. These 3D computations also confirm that the temperature field is almost uniform in the transverse direction over a major part of the cavity.

The model we propose is based on the averaging of the momentum, mass and heat conservation equations along the transverse dimension of the cavity, $\boldsymbol{x_3}$. To analytically compute the average, the temperature is assumed uniform along $\boldsymbol{x_3}$ and a well-defined shape must be chosen for the velocity profile. We show that choosing a profile featuring two boundary layers of thickness δ and a uniform bulk is more appropriate than choosing a parabolic Poiseuille profile. The thickness δ is a tunable parameter. We choose it uniform on the 2D domain. For a given fluid, which is to say at fixed Prandtl number value, the value of δ is optimized so as to minimize the mean deviation between the 3D and the 2D½ temperature fields at an intermediate Grashof number value. We show that the 2D½ model featuring this value of boundary layer thickness δ is efficient over more than one decade in terms of Grashof number. The mean deviation over the 2D domain between the 2D½ and the 3D temperature fields is typically less than 2% of the longitudinal temperature difference, $\Delta\theta$. The maximum local deviation stays below 10% in the considered range of parameters. The simulations made with this 2D½ model are observed to be more than 20 times less time-consuming than the 3D calculations (with the same grid in constant-x_3 planes).

Finally, original experimental results are reported and used as a test case for the numerical calculations. It is shown that both the 2D½ and 3D calculations correctly reproduce the experimental temperature measurements.

As a perspective, this type of models could be used to simulate solidification experiments, both for pure liquid metals and for metallic alloys. This would offer the opportunity of doing extensive parametric studies, possibly with a very fine meshing of the 2D domain, at a reasonable cost in terms of computational time.

Acknowledgements

Funding for this project was provided by a grant from La Région Rhône-Alpes.

References

[1] X.D. Wang, P. Petitpas, C. Garnier, J.P. Paulin, Y. Fautrelle, Comptes Rendus Mécanique 335 (2007) 336–341.
[2] X.D. Wang, Y. Fautrelle, International Journal of Heat and Mass Transfer 52 (2009) 5624–5633.
[3] L. Hachani, B. Saadi, X.D. Wang, A. Nouri, K. Zaidat, A. Belgacem-Bouzida, L. Ayouni-Derouiche, G. Raimondi, Y. Fautrelle, International Journal of Heat and Mass Transfer 55 (2012) 1986–1996.
[4] R. Boussaa, O. Budenkova, L. Hachani, X.D. Wang, B. Saadi, K. Zaidat, H. Ben Hadid, Y. Fautrelle, in: CFD Modeling and Simulation in Materials Processing, John Wiley & Sons, Inc., Hoboken, NJ, USA, 2012, pp. 163–170.
[5] L. Hachani, R. Boussaa, B. Saadi, X.D. Wang, K. Zaidat, A. Belgacem-Bouzida, D. Henry, V. Botton, H. Ben Hadid, Y. Fautrelle, in: Proceedings 7th International Conference on Electromagnetic Processing of Materials (Beijing, China), 2012, pp. 286–290.
[6] H.J.S. Hele-Shaw, Nature 98 (1898) 34.
[7] H. Schlichting, K. Gersten, Boundary Layer Theory, eighth revised and enlarged ed., Springer, New York, 2000.
[8] H. Ockendon, J.R. Ockendon, Viscous Flow, Cambridge University Press, 1995.
[9] P. Gondret, M. Rabaud, Physics of Fluids 9 (1997) 3267–3274.
[10] C. Ruyer-Quil, Comptes Rendus de l'Académie des Sciences, Series IIb: Mecanique 329 (2001) 337–342.
[11] D. Bensimon, L.P. Kadanoff, S. Liang, B.I. Shraiman, C. Tang, Reviews of Modern Physics 58 (1986) 977–999.
[12] G.M. Homsy, Annual Review of Fluid Mechanics 19 (1987) 271–311.
[13] S.B. Savage, K. Hutter, Journal of Fluid Mechanics 199 (1989) 177–215.
[14] M. Böckmann, S.C. Müller, Physical Review Letters 85 (2000) 2506–2509.
[15] J. Huang, B.F. Edwards, Physical Review E 54 (1996) 2620–2627.
[16] R.F. Katz, M.G. Worster, Journal of Computational Physics 227 (2008) 9823–9840.
[17] R.T. Deam, B. Bednarz, N. Stokes, Modelling and Simulation in Materials Science and Engineering 13 (2005) 471–492.
[18] V.T. Chow, Open-channel Hydraulics, McGraw-Hill International Editions, 1973.
[19] R.J. Moreau, Magnetohydrodynamics, Kluwer, The Netherlands, 1990.
[20] C.J. Smithells, E.A. Brandes, Smithells Metals Reference Book, sixth ed., Butterworths, 1983.